Degrees of Freedom and Characteristic Modes

Gustafsson, Mats; Lundgren, Johan

2023

CODEN:LUTEDX/(TEAT-7276)/1-21/(2023)

Degrees of Freedom and Characteristic Modes

M. Gustafsson and J. Lundgren

Electromagnetic Theory
Department of Electrical and Information Technology
Lund University
Sweden

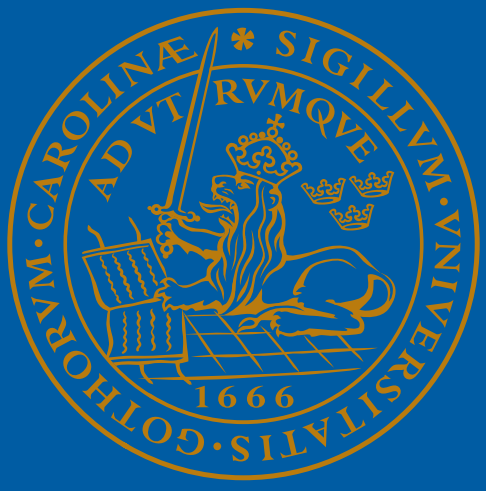

(TEAT-7276)/1-21/(2023): M. Gustafsson and J. Lundgren, Degrees of Freedom and Characteristic Modes

Mats Gustafsson
mats.gustafsson@eit.lth.se

Department of Electrical and Information Technology
Electromagnetic Theory
Lund University
P.O. Box 118
SE-221 00 Lund
Sweden

Johan Lundgren
johan.lundgren@eit.lth.se

Department of Electrical and Information Technology
Electromagnetic Theory
Lund University
P.O. Box 118
SE-221 00 Lund
Sweden

This is an author produced preprint version as part of a technical report series from the Electromagnetic Theory group at Lund University, Sweden. Homepage `https://www.eit.lth.se` and `https://portal.research.lu.se`.

Editor: Mats Gustafsson

Abstract

The number of degrees of freedom is a crucial parameter in many electromagnetic problems. In for example modern communication systems spatial diversity is often employed through multiple beams to enhance capacity and reliability. However, while the degrees of freedom can be computed, their connection to physical quantities is not as easily understood. To address this issue, this paper proposes a scattering-based formulation of characteristic mode analysis that can estimate the degrees of freedom of arbitrarily-shaped objects. The relation between the number of dominant characteristic modes and physical characteristics differs for electrically large and small objects. Specifically, for large objects, it is linked to the average shadow area, while for small objects, it is linked to their average polarizability through the forward scattering sum rule. Therefore, the average shadow area and polarizability are fundamental parameters that provide insight into the number of degrees of freedom for any object. These basic parameters also provide straightforward estimates of the minimum size of a device region required to support a desired number of electromagnetic degrees of freedom across a given spectral response.

1 Introduction

Electromagnetic degrees of freedom (DoF) are fundamental in the design and optimization of antennas, wireless communication systems, and electromagnetic scattering problems [2, 8, 9, 10, 22, 23, 28, 29, 31]. The number of DoF (NDoF) determines the degree of adjustability available to achieve a desired level of performance. For example, in antenna design, a larger NDoF allows for greater control over the radiation pattern and maximum directivity [23]. Similarly, in wireless communication systems, the NDoF is linked to the number of available channels or spatial dimensions that can be employed to transmit signals (multiplexing), resulting in higher data rates, and improved reliability in technologies such as multiple-input multiple-output (MIMO) systems [28, 33] and intelligent surfaces [32]. In the context of electromagnetic scattering, the NDoF is associated with the control of scattering and radar cross-sections [2]. Overall, NDoF is a crucial parameter that plays a fundamental role in a range of electromagnetic applications.

In electromagnetic systems, the NDoF typically increases with the electrical size of the object under consideration. For instance, smaller antennas tend to have fewer DoF and lower directivity, whereas larger antenna arrays can have many DoF and consequently much higher directivity [23]. Classical estimates of the NDoF rely on canonical geometries and modal expansions, such as spherical wave expansions and propagating modes in waveguides [2, 28, 29], which are briefly revisited in this paper. To complement these estimates, modal expansion and numerical evaluations based on eigenvalue and singular-value decompositions are used [8, 31]. In other non-canonical systems, such as antenna structures, characteristic mode (CM) analysis is employed to identify resonant modes, which, along with their orthogonal radiation patterns, provide valuable insights into available NDoF for multiple-input and multiple-output (MIMO) antenna systems [3, 5, 26].

In this paper, a combination of scattering theory and characteristic mode analysis is proposed as a means of estimating the NDoF of arbitrarily shaped objects. The NDoF is determined from the number of significant CMs, *i.e.*, modes with characteristic values $|\lambda_n| \leq 1$ [5]. The scattering-based formulation of CM analysis [16] is used to determine the DoF of arbitrarily-shaped objects. Combining CM expansion with the extinction paradox (shadow scattering) [30] demonstrates that the average shadow area provides an estimate of the number of significant characteristic modes for electrically large objects. This leads to a simple estimate of the NDoF generalizing classical estimates [2, 8, 23, 28, 29, 31] based on spherical wave expansions, waveguide theory, and numerical techniques to a simple closed-form expression for arbitrarily shaped regions. For smaller electrical sizes, the NDoF available, over a bandwidth, is linked to the average polarizability of the structure through the forward scattering sum rule [12, 36, 37].

The average shadow area and average polarizability are fundamental parameters for analyzing the DoF and provide insight into the NDoF for arbitrarily shaped objects. Additionally, they offer straightforward estimates of the minimum size of a device region required to support a desired NDoF over a given spectral response. This paper explores the use of these parameters and demonstrates how they can be employed. We begin with a general overview of DoF and canonical systems in Sec. 2, followed by an introduction of CM analysis into DoF in Sec. 3. In Sec. 4 the modal significance is connected to the scattering cross-section. The average shadow area is then utilized in Sec. 5 to estimate the number of dominant CM. For smaller, and bandwidth-restricted devices, the average polarizability is employed in Sec. 6 to achieve similar result. Finally, in Sec. 7 we offer insights into how this can be used to estimate the minimum required size for a specific NDoF. The paper is concluded in Sec. 8.

2 Degrees of freedom

The continuous nature of space and time requires an infinite number of modes to expand a field or equivalently a continuous set of points to sample a field. Although there is an infinite number of modes, it is often sufficient to consider a finite number of them for a required accuracy. These finite number of modes represent the DoF and the NDoF quantifies how many independent parameters that in practice are needed to represent a field for a given application. The NDoF for signals is often determined from the dominant term of the time-bandwidth product [10, Chap. 1]. DoF has *e.g.*, been used to analyze imaging [7, 31], communication [18, 28, 32, 33], and antenna systems [6, 23]. For time-harmonic cases, the NDoF can be obtained from analytic mode expansions of canonical objects [23] or numerically using singular value decomposition [31].

DoFs for the interaction between a time-harmonic electromagnetic field at a wavenumber k and an object, are classically analyzed using mode expansions for canonical geometries [2, 23, 28, 29, 31] and more recently radiation modes [8] for arbitrary shapes. Waveguide modes, see Box 1, have a distinct characterization of

Box 1. Degrees of freedom and waveguide modes

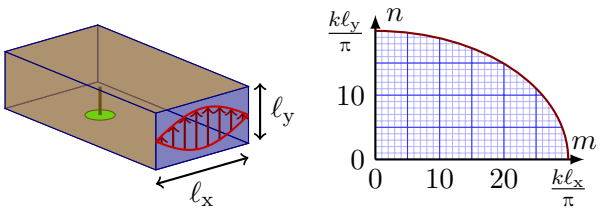

The rectangular waveguide, characterized by its side lengths ℓ_x and ℓ_y possesses finite number of propagating modes [34]

$$k^2 - \frac{m^2\pi^2}{\ell_x^2} - \frac{n^2\pi^2}{\ell_y^2} \geq 0 \Rightarrow \frac{m^2\pi^2}{k^2\ell_x^2} + \frac{n^2\pi^2}{k^2\ell_y^2} \leq 1, \tag{B.1}$$

with non-negative integers m and n. The inequality presented in (B.1) describes a quarter ellipse whose area approximately is the number of propagating modes. Waveguide modes are divided into transverse electric (TE), with indices $\max\{m,n\} \geq 1$, and transverse magnetic (TM), with $\min\{m,n\} \geq 1$, both of which are described by (B.1). The total number of modes for the waveguide is approximated by two (TE and TM) times the area of the quarter ellipse

$$N_A \approx 2\frac{\pi}{4}\frac{k^2\ell_x\ell_y}{\pi^2} = \frac{k^2A}{2\pi} \quad \text{for } k\min\{\ell_x,\ell_y\} \gg 1, \tag{B.2}$$

where $A = \ell_x\ell_y$ is the physical cross-section area of the waveguide.

propagating and evanescent modes, with the propagating modes contributing to the DoF. For radiating systems enclosed by a sphere, there is no similar characterization, and we have to use a threshold level to define propagating modes and the DoF, see Box. 2.

Both these analytically solvable cases have approximately $N_A \approx k^2A/(2\pi)$ degrees of freedom for a surface area A in the electrically large limit. Does this hold for other shapes? Could the area of an object somehow be used to estimate its NDoF? A direct complication is to define the area for general shapes. While it is easy to synthesize objects with a large surface area by *e.g.*, folding the structure, this is unlikely to increase the NDoF. Using the area of the convex hull is more stable, but faces problems for disjoint objects.

With this idea as a starting point, we use CM to investigate the NDoF of objects. For electrically large structures we show that there is an area-related quantity of interest that is fundamentally linked to the NDoF, the average shadow area. The average shadow area is a fathomable quantity providing insights into electrically larger objects. However, there is merit in observing smaller objects for which this estimate does not accurately estimate the NDoF. There is another quantity, the average polarizability, which can describe electrically smaller objects' NDoF and even resonant behaviors through bandwidth limitations and the forward scattering sum rule.

Box 2. Degrees of freedom and spherical modes

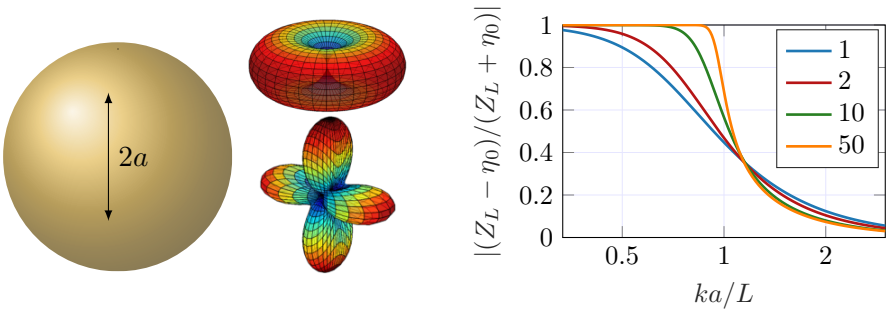

Consider a sphere of radius a. A classical approach to estimate the DoF for radiating systems (antennas) is to expand the propagating field in spherical waves [25, 39], such as the dipoles and quadrupole radiation patterns illustrated in the middle of the top of the box. There is an infinite number of spherical waves and no distinct cut-off as with a rectangular waveguide in Box 1, but contributions from waves with degree $L > ka$ diminishes rapidly [19], as *e.g.*, illustrated by the miss-match between spherical waves and free-space waves in the top right of the Box. This suggests a cutoff $L \approx ka$ and a total number of $N_{\mathrm{A}} \approx 2L(L+2)$ dominant modes giving $N_{\mathrm{A}} \leq 6$ for $ka \ll 1$ and

$$N_{\mathrm{A}} \approx 2L^2 \approx 2(ka)^2 = \frac{k^2 A}{2\pi} \quad \text{for } ka \gg 1, \tag{B.3}$$

where $A = 4\pi a^2$ is the surface area of the sphere. Although, this simple estimate is often preferable, improved estimates are valuable in *e.g.*, near-field measurements and computational techniques [38].

3 DoF and Characteristic modes

Describing the NDoF for general systems is not a trivial task. For canonical systems such as the waveguide, Box 1, or the sphere, Box 2, a connection between propagation modes and physical parameters are not too complicated. A general antenna system does not fall directly into any of these categories, yet similar physical insight can be obtained. To begin describing any object and attempts to formulate a radiation basis we turn to the popular tool in antenna and scattering theory, characteristic mode analysis, see Box 3. This technique is partly motivated by extending good properties from Mie theory for spherical geometries to arbitrary shapes. Characteristic values $\lambda_n = 0$ indicate resonant modes and the distance to resonance is typically quantified by the modal significance

$$|t_n| = \frac{1}{\sqrt{1+\lambda_n^2}}, \tag{3.1}$$

where $0 \leq |t_n| \leq 1$ and $|t_n| = 1$ for resonant modes. The number of CMs is infinite, but the impact of high-order modes having low modal significance decreases rapidly, similar to the spherical waves in Box 2. This is *e.g.*, seen in the classical summation

Box 3. Characteristic modes

Characteristic mode (CM) analysis is a popular tool for antenna analysis [3, 5]. CM is often based on method-of-moments (MoM) matrices as proposed by Harrington and Mautz [20] and defined as an eigenvalue decomposition of the MoM matrix, $\mathbf{Z} = \mathbf{R} + \mathrm{j}\mathbf{X}$, according to [20]

$$\mathbf{X}\mathbf{I}_n = \lambda_n \mathbf{R}\mathbf{I}_n \Leftrightarrow \mathbf{Z}\mathbf{I}_n = (1 + \mathrm{j}\lambda_n)\mathbf{R}\mathbf{I}_n. \tag{B.4}$$

Scattering-based formulations of CM were originally proposed by Garbacz [11] and are based on an eigenvalue decomposition of a scattering operator, *e.g.*, spherical-wave scattering with the transition matrix $\mathbf{T}$ [16] or plane-wave scattering with a scattering dyadic $\boldsymbol{S}$ [4, 25] and integral operator $\widetilde{\boldsymbol{S}}$

$$\widetilde{\boldsymbol{S}}\boldsymbol{F}_n = \frac{-\mathrm{j}k}{4\pi} \int_{4\pi} \boldsymbol{S}(\hat{\boldsymbol{r}}, \hat{\boldsymbol{r}}') \cdot \boldsymbol{F}_n(\hat{\boldsymbol{r}}') \, \mathrm{d}\Omega' = t_n \boldsymbol{F}_n(\hat{\boldsymbol{r}}), \tag{B.5}$$

where the eigenvalue t_n is related to λ_n through $t_n = -1/(1 + \mathrm{j}\lambda_n)$. The modal far-fields $\boldsymbol{F}_n(\hat{\boldsymbol{r}})$ are orthogonal $\frac{1}{4\pi}\int_{4\pi} \boldsymbol{F}_m^* \cdot \boldsymbol{F}_n \, \mathrm{d}\Omega = \delta_{mn}$. Modes with characteristic values $\lambda_n = 0$ or equivalently $t_n = -1$ are resonant and modal significance $|t_n| = 1/\sqrt{1 + \lambda_n^2}$ is used to quantify the potential impact of a mode [3].

formula based on the characteristic currents $\mathbf{I}_n$ in (B.4) for a current $\mathbf{I}$ induced by an excitation $\mathbf{V}$ [20]

$$\mathbf{I} = \sum_n \frac{\mathbf{I}_n^{\mathrm{T}}\mathbf{V}}{1 + \mathrm{j}\lambda_n}\mathbf{I}_n, \tag{3.2}$$

which can be interpreted as a low-pass structure in $|\lambda_n|$ with cutoff $|\lambda_n| = 1$. CMs with small $|\lambda_n|$ can often be tuned to resonance and modes with

$$|\lambda_n| \leq 1 \Longleftrightarrow |t_n|^2 \geq 1/2, \tag{3.3}$$

are termed significant modes [5]. In this paper, we determine the NDoF for electrically large lossless objects from the number of significant characteristic modes (3.3).

The number of significant characteristic modes for the PEC objects in Fig. 1 is depicted by solid curves in Fig. 2 for electrical sizes $ka \in [1, 20]$, where a is the radius of the smallest circumscribing sphere. We observe that the number of significant modes oscillates around the (dashed) lines with slope $(ka)^2$, *i.e.*, as the electrical size squared similar to the often used number of relevant spherical modes $N \approx 2(ka)^2$ for $ka \gg 1$, see Box 2. These dashed lines depend solely on the geometrical shape which is presented in detail in Sec. 5. The curves differ for smaller sizes where the number of CMs depends on resonances as discussed in Sec. 6.

4 Scattering cross-section and modal significance

Similar to the CMs, the scattering of electromagnetic waves is a an inherent property of how a specific object interacts and can be utilized to estimate the number

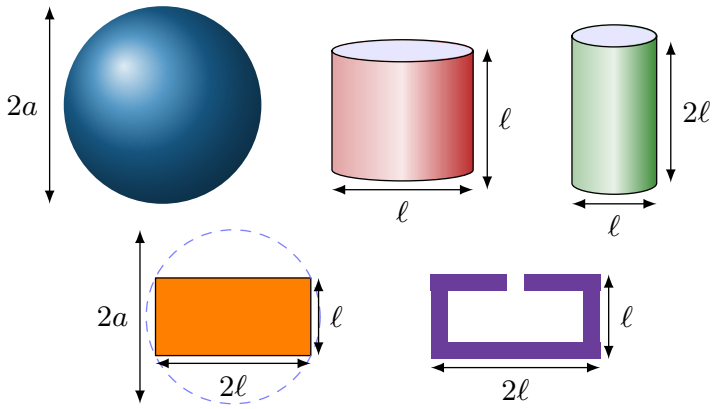

Figure 1: Investigated PEC objects: sphere (blue), open cylinder, no top or bottom surface, with equal height and diameter (red), open cylinder with height two times the diameter (green), planar rectangle with side lengths ℓ and 2ℓ (orange), and split ring resonator (SRR) of width $\ell/5$ and with side lengths ℓ and 2ℓ (purple). All dimensions are normalized to the radius a of the smallest circumscribing sphere, as indicated by the dashed circle around the rectangle.

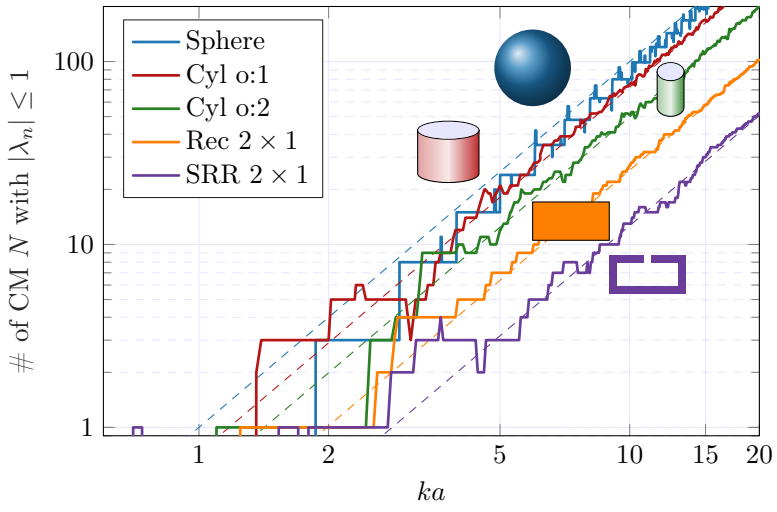

Figure 2: Number of significant characteristic modes ($|\lambda_n| \leq 1$) for the five PEC objects (solid lines) in Fig. 1 compared with estimates from (5.2) (dashed lines).

Box 4. Scattering cross section

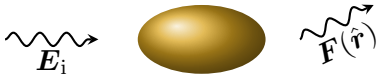

The scattering cross section σ_{s} is defined as the scattered power normalized with the incident power density according to

$$\sigma_{\mathrm{s}}(\hat{\boldsymbol{k}}, \hat{\boldsymbol{e}}) = \frac{1}{|\boldsymbol{E}_0|^2} \int_{4\pi} |\boldsymbol{F}(\hat{\boldsymbol{r}})|^2 \, \mathrm{d}\Omega_{\hat{\boldsymbol{r}}} \tag{B.6}$$

for an incident plane wave $\boldsymbol{E}_{\mathrm{i}}(\boldsymbol{r}) = \boldsymbol{E}_0 \mathrm{e}^{-\mathrm{j}k\hat{\boldsymbol{k}}\cdot\boldsymbol{r}}$ in the direction $\hat{\boldsymbol{k}}$ with polarization $\hat{\boldsymbol{e}} = \boldsymbol{E}_0/|\boldsymbol{E}_0|$ and where $\boldsymbol{F}(\hat{\boldsymbol{r}})$ denotes the scattered far field.

of significant modes. The scattering formulation of CM relates a total modal significance to the scattering cross-section, see Box 4. The modal significance squared, $|t_n|^2$, is proportional to the scattered power [16] and is related to the scattering cross-section's σ_{s}, average over illumination directions and polarizations through [25]

$$\langle \sigma_{\mathrm{s}} \rangle = \frac{1}{8\pi^2} \int_{4\pi} \int_{2\pi} \sigma_{\mathrm{s}}(\hat{\boldsymbol{k}}, \hat{\boldsymbol{e}}) \, \mathrm{d}\Omega_{\hat{\boldsymbol{e}}} \, \mathrm{d}\Omega_{\hat{\boldsymbol{k}}} = \frac{2\pi}{k^2} \sum_n |t_n|^2, \tag{4.1}$$

where $\hat{\boldsymbol{k}}$ and $\hat{\boldsymbol{e}}$ denote the direction and polarization of the incident wave, see Box. 4. The sum of squared modal significance is identified with the Frobenius norm of the transition matrix, $\mathbf{T}$, or scattering dyadic operator, $\widetilde{\boldsymbol{S}}$,

$$\sum_n |t_n|^2 = \|\mathbf{T}\|_{\mathrm{F}}^2 = \|\widetilde{\boldsymbol{S}}\|_{\mathrm{F}}^2. \tag{4.2}$$

The identity, (4.1), shows that prior knowledge of the average scattering cross-section determines an upper bound on the number of resonant ($|t_n| = 1$), or significant ($|t_n|^2 \geq 1/2$) characteristic modes. The identity (4.1) can also be interpreted from forward scattering and the optical theorem by identifying the scattering and extinction cross section for lossless objects [25].

Shadow scattering [30] (or extinction paradox), see Box 5, for a lossless object demonstrates that the scattering cross-section σ_{s} of an object approaches twice the shadow cross-sectional area $A_{\mathrm{s}}(\hat{\boldsymbol{k}})$, *i.e.*,

$$\sigma_{\mathrm{s}}(\hat{\boldsymbol{k}}, \hat{\boldsymbol{e}}) \approx 2A_{\mathrm{s}}(\hat{\boldsymbol{k}}) \quad \text{as } ka \to \infty. \tag{4.3}$$

Averaging over all directions $\hat{\boldsymbol{k}}$ and polarizations $\hat{\boldsymbol{e}}$ relates the average scattering cross-section and total modal significance with the average shadow area

$$\langle \sigma_{\mathrm{s}} \rangle \approx 2\langle A_{\mathrm{s}} \rangle = \frac{1}{4\pi} \int_{4\pi} 2A_{\mathrm{s}}(\hat{\boldsymbol{k}}) \, \mathrm{d}\Omega_{\hat{\boldsymbol{k}}} \approx \frac{2\pi}{k^2} \sum_n |t_n|^2. \tag{4.4}$$

This relates a geometrical property, interpreted as the average shadow area $\langle A_{\mathrm{s}} \rangle$ of the obstacle, to the electromagnetic response, the sum of modal significances. For a

Box 5. Average shadow area

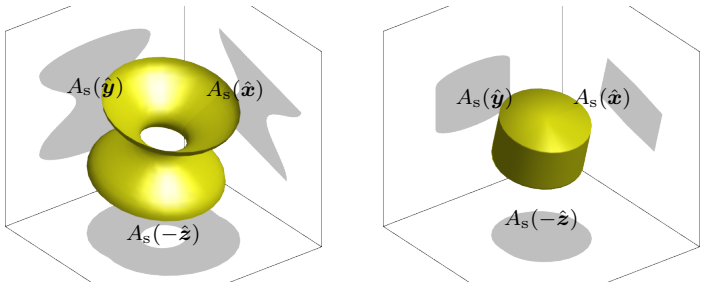

Shadow areas $A_s(\hat{\boldsymbol{k}})$ for a non-convex object (left) and a convex object (right) illuminated for the perpendicular directions $\hat{\boldsymbol{x}}, \hat{\boldsymbol{y}}, \hat{\boldsymbol{z}}$. The average shadow area is computed by considering all incident illumination directions,

$$\langle A_s \rangle = \frac{1}{4\pi} \int_{4\pi} A_s(\hat{\boldsymbol{k}}) \, \mathrm{d}\Omega_{\hat{\boldsymbol{k}}}. \tag{B.7}$$

It simplifies for convex objects with the surface area A as shown by A. Cauchy, see *e.g.*, [40], to

$$\langle A_s \rangle = \frac{1}{4\pi} \int_{4\pi} \int_{\Omega} \frac{|\hat{\boldsymbol{k}} \cdot \hat{\boldsymbol{n}}|}{2} \, \mathrm{dS} \, \mathrm{d}\Omega_{\hat{\boldsymbol{k}}} = \frac{1}{4} \int_{\Omega} \mathrm{dS} = \frac{A}{4}, \tag{B.8}$$

where Ω denotes the surface region of the object and $\hat{\boldsymbol{n}}$ is the outward unit normal. Similarly, the average shadow area for planar objects (*e.g.*, a PEC surface in the xy-plane) is $\langle A_s \rangle = A/2$, which is consistent with (B.8) if the area of the two sides is considered. The average shadow area for a convex object is also bounded by the maximal geometrical cross-sectional area

$$\frac{1}{2} \max_{\hat{\boldsymbol{k}}} A_s(\hat{\boldsymbol{k}}) \leq \langle A_s \rangle \leq \max_{\hat{\boldsymbol{k}}} A_s(\hat{\boldsymbol{k}}), \tag{B.9}$$

with equality to the left and right for planar and spherical objects, respectively.

convex object this average shadow area is related to the surface area A in a straightforward fashion, see Box 5. Average shadow areas for the convex and non-convex objects in Fig. 1 are presented in Tab. 1.

Shadow scattering provides accurate estimates (4.4) of the scattering cross-section for electrically large objects, but the estimate breaks down for smaller objects, calling for other approximations. Here, we use that scattering of electrically small objects is described by Rayleigh (dipole) scattering, see Box 6, with scattering cross-section

$$\langle \sigma_s \rangle = \frac{2\pi}{k^2} \sum_n |t_n|^2 \approx \frac{k^4 \langle \gamma^2 \rangle}{6\pi}, \tag{4.5}$$

where $\langle \gamma^2 \rangle = \langle \boldsymbol{\gamma}_e^2 + \boldsymbol{\gamma}_m^2 \rangle = \frac{1}{3} \mathrm{Tr}\{\boldsymbol{\gamma}_e^2 + \boldsymbol{\gamma}_m^2\}$ denotes the average squared polarizability dyadic, see Tab. 1. Intersection of the low-(4.5) and high-frequency (4.4) limits $\langle \sigma_s \rangle = 2\langle A_s \rangle$ propose a unification by scaling the average scattering cross-section

					
$\langle A_\mathrm{s}\rangle/a^2$	3.14	2.27	1.56	0.80	0.40
$\langle\gamma\rangle/a^3$	6.28	4.06	2.71	1.35	1.55
$\sqrt{\langle\gamma^2\rangle}/a^3$	14.0	7.37	4.98	2.25	2.14
$k_\mathrm{a}a$	0.88	1.12	1.23	1.56	1.35

Table 1: Average shadow area $\langle A_\mathrm{s}\rangle$, polarizability $\langle\gamma\rangle$, squared polarizability $\langle\gamma^2\rangle$, and cut-off radius $k_\mathrm{a}a$ for the PEC objects in Fig. 1. All parameters are normalized by the radius, a, of the smallest circumscribing sphere.

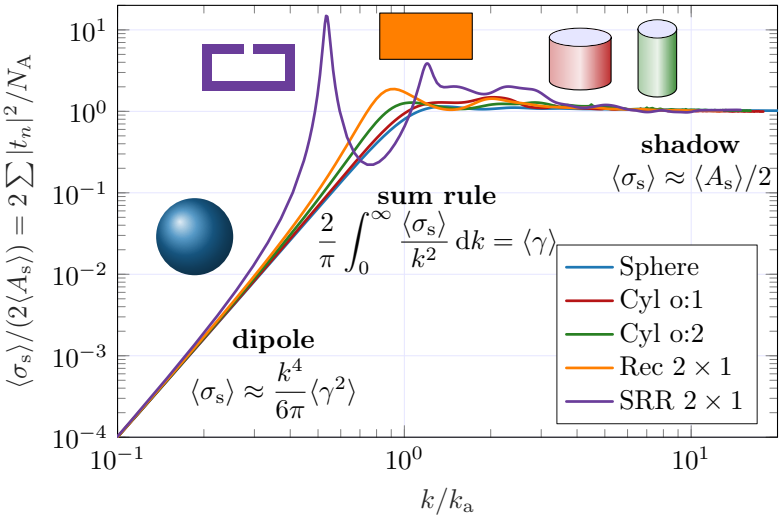

Figure 3: Average scattering cross sections $\langle\sigma_\mathrm{s}\rangle$ for the objects in Fig. 1 normalized by two times the average shadow area $\langle A_\mathrm{s}\rangle$ and function of the normalized wavenumber k/k_a.

with the double average shadow area and the wavenumber according to

$$k_\mathrm{a} = \sqrt[4]{\frac{12\pi\langle A_\mathrm{s}\rangle}{\langle\gamma^2\rangle}}. \tag{4.6}$$

This scaling transforms the Rayleigh limit (4.5) to a straight line (in a log-log diagram) with slope k^4 crossing the point $(1, 1)$, see Fig. 3 and unifies the average scattering cross section to approximate an ideal high-pass filter

$$\langle\sigma_\mathrm{s,i}\rangle = \min\{(k/k_\mathrm{a})^4, 1\} \tag{4.7}$$

with cutoff k_a. The different objects in Fig. 3 have average scattering cross-sections $\langle\sigma_\mathrm{s}\rangle$ close to the straight-line approximation with the largest deviations around $k \approx k_\mathrm{a}$ as mostly apparent for the SRR.

The normalization k/k_a reduces to approximately ka for many objects, see Tab. 1, but can differ greatly for other objects such as two separated spheres.

Box 6. Rayleigh (dipole) scattering

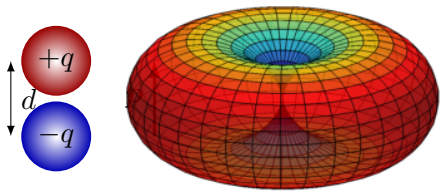

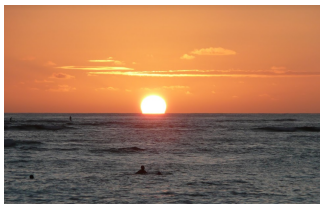

Rayleigh scattering is the dominant scattering contribution for objects much smaller than the wavelength and *e.g.*, explaining the color of the sky [1, 21]. The scattered field by an electrically small object can be described as radiation from electric and magnetic dipoles. Polarizability dyadics $\boldsymbol{\gamma}_\mathrm{e}$ and $\boldsymbol{\gamma}_\mathrm{m}$ are defined by dipole scattering with electric $\boldsymbol{p}$ and magnetic $\boldsymbol{m}$ dipole moments [1, 21, 24],

$$\boldsymbol{p} = \varepsilon_0 \boldsymbol{\gamma}_\mathrm{e} \cdot \boldsymbol{E}_\mathrm{i} \quad \text{and} \quad \boldsymbol{m} = \boldsymbol{\gamma}_\mathrm{m} \cdot \boldsymbol{H}_\mathrm{i}. \tag{B.10}$$

The electric polarizability dyadic, $\boldsymbol{\gamma}_\mathrm{e}$, is determined from the first moment of the induced charge density on the object when placed in a constant electrostatic field [15, 24]. A charge distribution on a rectangular PEC plate is depicted to the right, where the typical accumulation of charges on edges and corners are seen [17]. Magnetic polarizability dyadic, $\boldsymbol{\gamma}_\mathrm{m}$, is associated with loop currents and is typically negative definite on PEC structures. They have the dimension of volume (m^3), but are not easily related to the physical volume, as illustrated by the PEC plate having zero volume and non-zero polarizability.

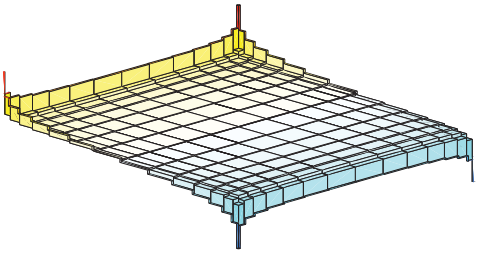

For a dielectric high contrast sphere with radius a, we have $\gamma = 4\pi a^3$ giving $k/k_\mathrm{a} = \sqrt[4]{4/3}ka \approx 1.07ka$ and a PEC sphere has $k/k_\mathrm{a} = \sqrt[4]{3/4}ka \approx 0.93ka$. Note that the discussed scaling is valid for lossless objects and that losses modify the low-frequency expansion [24].

5 Number of dominant CM and shadow scattering

Combining the average scattering cross section (4.1) with shadow scattering (4.4) shows that the total modal significance is proportional to the average shadow area

$$\sum_n |t_n|^2 = \frac{k^2}{2\pi}\langle \sigma_\mathrm{s} \rangle \approx \frac{k^2}{\pi}\langle A_\mathrm{s} \rangle, \tag{5.1}$$

for electrically large obstacles $ka \gg 1$. The relation (5.1) directly produces an upper limit on the number of resonance modes $|t_n| = 1$ but in general, not all modes are resonant, and it is more relevant to estimate the number of approximately resonance

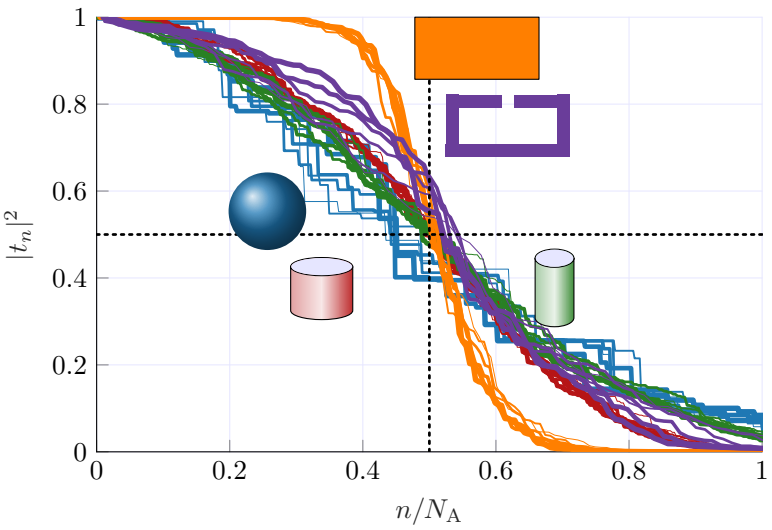

Figure 4: Eigenvalue amplitudes $|t_n|^2$ for $ka \in [15, ..., 20]$ indicated by increasing line widths. The horizontal axis is a scaled mode index n/N_{A} for $n = 1, 2, \ldots, N_{\mathrm{A}}$.

modes, here defined as significant modes (3.3), *i.e.*, $|t_n|^2 \geq 1/2$ or equivalently $|\lambda_n| \leq 1$, giving the bound

$$N \lessapprox N_{\mathrm{A}} = \frac{2k^2\langle A_{\mathrm{s}}\rangle}{\pi} \overset{\text{convex object}}{=} \frac{k^2 A}{2\pi}, \tag{5.2}$$

for $k \gg k_{\mathrm{a}}$. This bound is identical to the classical DoF estimate for waveguide modes in Box 1 and spherical waves in Box 2 for convex objects.

Limit (5.2) is unrealistic as it assumes that all N modes have $|\lambda_n| = 1$, when in reality the eigenvalues are distributed in $[-\infty, \infty]$. Distributions of modal significances for the five considered obstacles are depicted in Fig. 4 for electrical sizes $ka \in [15, ..., 20]$, with squared modal significance $|t_n|^2$ as the vertical axis and normalized mode index n/N_{A} as the horizontal axis. This normalization together with the total modal significance (5.1) leads to the interpretation that the area under a curve is approximately $1/2$, as confirmed by inspection of the curves. The curves also indicate an approximate mirror symmetry around the point $(1/2, 1/2)$. This symmetry is verified for a sphere with $ka = 1000$ and rectangle and SRR with $ka = 100$ in Fig. 5, where the dashed curves are mirror symmetrized curves but the (non-convex) open cylinders show that the curves are generally non-symmetric.

The intersection of the curves at $(1/2, 1/2)$ approximates the number of significant characteristic modes ($|\lambda_n| \leq 1$) to

$$N \approx \frac{N_{\mathrm{A}}}{2} = \frac{k^2\langle A_{\mathrm{s}}\rangle}{\pi}. \tag{5.3}$$

This estimate is illustrated for the objects in Fig. 1 by the dashed lines in Fig. 2 and Fig. 6. In Fig. 6, we observe that the curves oscillate around an approximately constant value. The relatively large oscillations for the sphere are linked to the

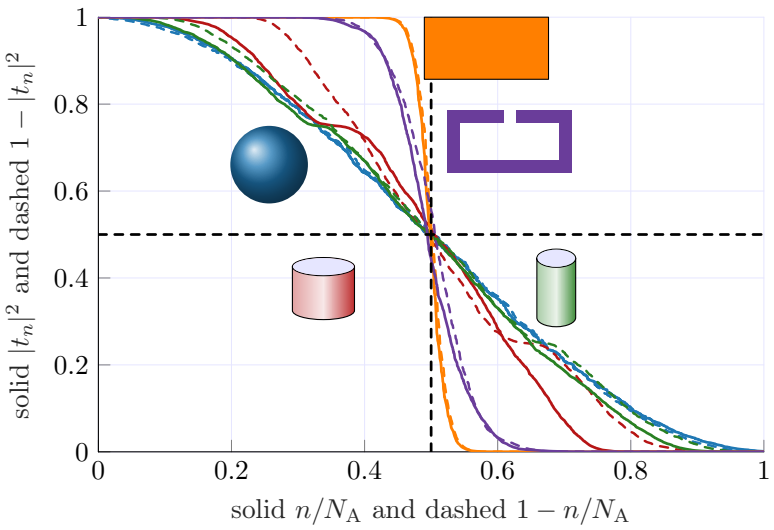

Figure 5: Eigenvalue amplitudes $|t_n|^2$ for electrically large cylinders, rectangle, SRR with $ka = 100$ and a sphere with $ka = 1000$ together with (dashed) symmetrized curves.

sphere symmetries, which effectively cancels the directional and polarization averaging in (4.1).

The sphere's surface area of $4\pi a^2$ gives $\langle A_{\mathrm{s}} \rangle = \pi a^2$ and $N \approx k^2 a^2$ which corresponds to the marker at 1/2 in Fig. 6. This means that on average, half of the modes from the classical spherical wave estimate $2(ka)^2$ in (B.3) are close to resonance. The other objects have smaller shadow areas and hence a lower number of significant modes. For example, the planar rectangle has surface area $2\ell^2 = 8a^2/5$ and average shadow area $\langle A_{\mathrm{s}} \rangle = 4a^2/5$ giving a marker at $2/(5\pi) \approx 0.13$, see Tab. 1. We observe that this is a very good estimate of the number of modes over the considered electrical sizes and objects, see Fig. 2. The average shadow area can hence be used to estimate the required size of an object for a desired NDoF.

6 Resonances and bandwidth restrictions

Shadow scattering estimate for the number of significant CMs (5.3) is accurate for $k \gg k_{\mathrm{a}}$ but do not provide any information for electrically smaller objects. Scattering in this electrically small range is better described by a set of resonances with $|t_n| = 1$. These resonances depend on the detailed structure of the object and are determined by solving the scattering problem numerically or analytically. Naturally, the number of resonant modes also requires a full wave solution of the scattering problem. Rayleigh scattering (4.5) show that the total modal significance

$$\|\mathbf{T}\|_{\mathrm{F}}^2 = \sum_n |t_n|^2 \approx \frac{k^6 \langle \gamma^2 \rangle}{12\pi^2}, \tag{6.1}$$

vanishes rapidly as the electrical size decreases $ka \to 0$, and hence that there are no

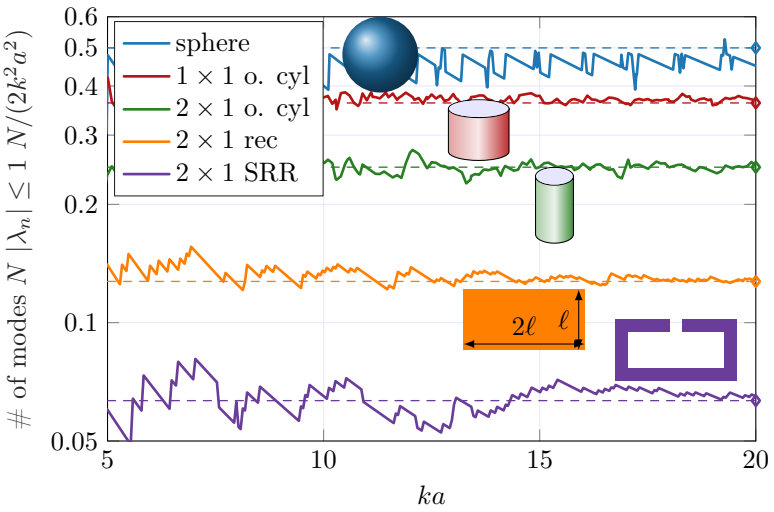

Figure 6: Number of characteristic modes with $|\lambda_n| \leq 1$ ($|t_n|^2 \geq 0.5$) for five objects normalized with the number of modes from a circumscribing sphere, $2k^2a^2$, in (B.3). Dashed lines and markers (at $ka = 20$) from average shadow area $\langle A_\mathrm{s} \rangle / (2\pi a^2)$

Box 7. Forward scattering sum rule

The forward scattering sum rule is an identity connecting all spectrum interaction between an object and a plane wave with the static interaction [12, 35]. The sum rule is *e.g.*, used to determine physical limitations in scattering and antenna theory [14, 37]. After averaging over directions and polarizations and assuming lossless obstacles, the sum rule reduces to

$$\frac{2}{\pi} \int_0^\infty \frac{\langle \sigma_\mathrm{s}(k) \rangle}{k^2} \, \mathrm{d}k = \langle \boldsymbol{\gamma}_\mathrm{e} + \boldsymbol{\gamma}_\mathrm{m} \rangle = \langle \gamma \rangle, \tag{B.11}$$

where $\boldsymbol{\gamma}_\mathrm{e}$ and $\boldsymbol{\gamma}_\mathrm{m}$ denote the static polarizability dyadics, see Box 6.

resonant modes for sufficiently small sizes. However, it is possible to synthesize objects with arbitrary low resonance frequencies. The bandwidths of these resonances are in general very narrow. Instead of estimating the number of resonant modes at a given frequency, we estimate the number of possible resonant modes over a bandwidth. These estimates are based on the forward scattering sum rule, see Box 7, here expressed in the total modal significance

$$\frac{2}{\pi} \int_0^\infty \frac{\langle \sigma_\mathrm{s}(k) \rangle}{k^2} \, \mathrm{d}k = 4 \sum_n \int_0^\infty \frac{|t_n(k)|^2}{k^4} \, \mathrm{d}k = \langle \gamma \rangle, \tag{6.2}$$

which relates the all spectrum modal significance with the average electric $\boldsymbol{\gamma}_\mathrm{e}$ and magnetic $\boldsymbol{\gamma}_\mathrm{m}$ polarizability dyadics $\langle \boldsymbol{\gamma}_\mathrm{e} + \boldsymbol{\gamma}_\mathrm{m} \rangle = \langle \gamma \rangle$. This implies that the total modal significance weighted with k^4 and integrated over all wavenumbers k is proportional to the trace of the static polarizability of the obstacle. This k^4 weight is identical to the case with realized gain [13, 36], where a resonance model is used to

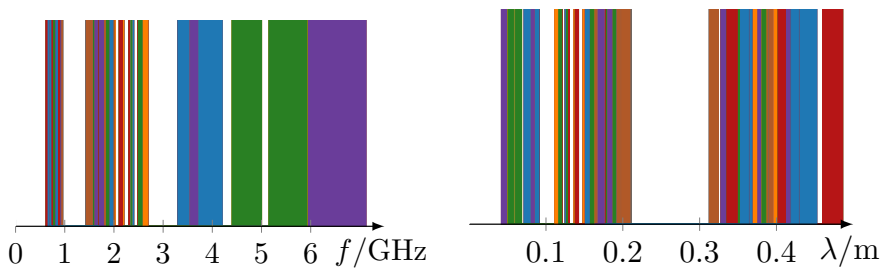

Figure 7: Illustration of the 5G spectrum with characteristic function χ_{5G} in frequency (left) and wavelength (right).

produce fundamental antenna limits and estimates of the bandwidth [13] and UWB onset frequency [36]. The sum rule is most interesting for electrically small objects due to the k^4 weight, where it shows that the average polarizability is fundamentally linked to the total modal significance over a bandwidth.

The sum rule identity (6.2) sets an upper bound on the total modal significance over all spectrum for a given polarizability and a lower bound on the polarizability for a desired spectral response. Consider a case with a desired number of resonant modes over a bandwidth. This requires a total modal significance greater than this number of resonant modes over the bandwidth. Introduce a desired spectral response $\chi(k)$ for which it is prescribed to have a total modal significance above $\chi(k)$, *i.e.*,

$$\sum_n |t_n(k)|^2 \geq \chi(k) \quad \text{for all } k. \tag{6.3}$$

The common simple case with a bandwidth interval $[k_1, k_2]$ having N resonant modes is given by the spectral response,

$$\chi_{[k_1,k_2]}(k) = \begin{cases} N & k_1 \leq k \leq k_2 \\ 0 & \text{otherwise.} \end{cases} \tag{6.4}$$

The desired spectral response is application specific and include more complex cases such as the 5G spectrum depicted in Fig. 7 with N resonant modes over the entire spectrum modeled by

$$\chi_{5G}(k) = \begin{cases} N & k \in \text{5G spectrum} \\ 0 & \text{otherwise.} \end{cases} \tag{6.5}$$

A lower bound on the average polarizability, $\langle\gamma\rangle_{\text{lb}}$, is obtained by evaluating the sum rule (6.2) with the desired spectral response

$$\langle\gamma\rangle_{\text{lb}} = 4\int_0^\infty \frac{\chi(k)}{k^4}\,\mathrm{d}k. \tag{6.6}$$

This is a fundamental limit on the polarizability $\langle\gamma\rangle \geq \langle\gamma\rangle_{\text{lb}}$ of an object to have a total modal significance (6.3).

Evaluating the sum rule for the constant spectral response over a finite bandwidth interval $k \in [k_1, k_2]$ in (6.4)

$$\langle \gamma \rangle_{\text{lb}} = 4 \int_{k_1}^{k_2} \frac{N}{k^4} \, \mathrm{d}k = \frac{4N}{3} \left(\frac{1}{k_1^3} - \frac{1}{k_2^3} \right). \tag{6.7}$$

For narrow bandwidths, it is practical to simplify the expression with the fractional bandwidth

$$B = \frac{k_2 - k_1}{k_0}, \tag{6.8}$$

around the center wavenumber $k_0 = (k_1 + k_2)/2$ transforming (6.7) to

$$\langle \gamma \rangle_{\text{lb}} \geq \frac{4BN}{k_0^3} \quad \text{or } N \leq \frac{k_0^3 \langle \gamma \rangle_{\text{lb}}}{4B}. \tag{6.9}$$

This shows that temporal diversity in the bandwidth B and spatial diversity in the number of modes N have similar effects on the polarizability of the object. For larger bandwidths, the general case (6.7) show that the contribution from the upper frequency reduces as $1 - k_1^3/k_2^3$ producing a difference of 8 % for $k_2 = 2k_1$ compared to an UWB case (6.10) with the onset wavenumber k_1 and upper wavenumber $k_2 = \infty$. This UWB case [36] simplifies to

$$\langle \gamma \rangle_{\text{lb}} = 4 \int_{k_1}^{\infty} \frac{N}{k^4} \, \mathrm{d}k = \frac{4N}{3k_1^3} \quad \text{or } N \leq \frac{3k_1^3 \langle \gamma \rangle_{\text{lb}}}{4}. \tag{6.10}$$

Consider as an example the 5G spectrum with a single mode $N = 1$ which by evaluating the sum rule (6.6) gives

$$4 \int_0^{\infty} \frac{\chi_{\text{5G}}}{k^4} \, \mathrm{d}k = \langle \gamma \rangle_{\text{lb}} \approx 456 \, \text{cm}^3, \tag{6.11}$$

implying that it is necessary to have an object with at least an average polarizability $\langle \gamma \rangle \geq 456 \, \text{cm}^3$ to be able to support the entire 5G spectrum. Instead using the UWB onset wavenumber corresponding to the lowest 5G frequency $f_1 \approx 0.62 \, \text{GHz}$ gives $4/(3k_1^3) \approx 618 \, \text{cm}^3$. This relatively small difference between considering the 5G spectrum and a UWB onset frequency emphasizes that the physical restrictions are dominated by the relatively small absolute bandwidth associated with the lowest frequencies. This is also better seen by plotting the 5G spectrum in wavelengths, as shown to the right in Fig. 7.

The total modal significance for an SRR is depicted in Fig. 8. A resonance around $ka \approx 0.7$ (or $f \approx 0.7 \, \text{GHz}$ for $2\ell \approx 8.5 \, \text{cm}$) has $\|\mathbf{T}\| \approx 1$ which is consistent with a dominant single ($N = 1$) dipole resonance. The low-frequency response approximates the Rayleigh limit (4.5) below the resonance, and the high-frequency response is close to the average shadow area (5.1) as indicated by the dashed lines. Sum rule bounds for UWB (6.10) and fractional bandwidth (6.9) have the same slope as the Rayleigh limit but include the potential for local resonances with a given bandwidth.

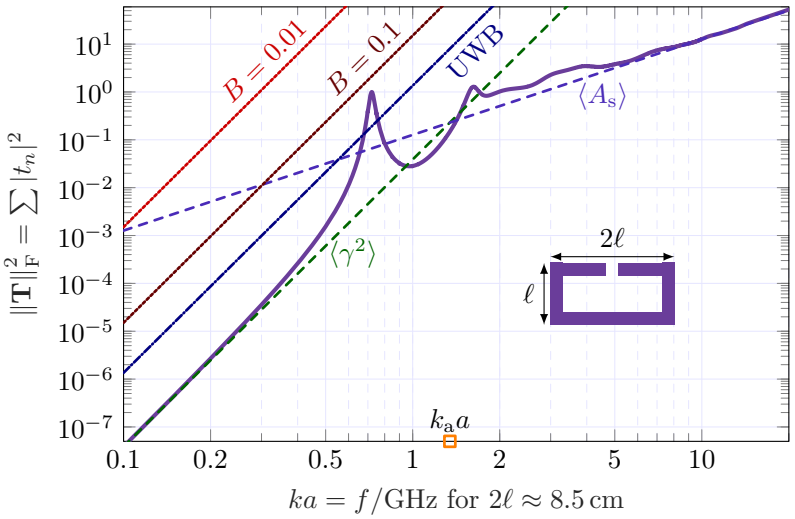

Figure 8: Total modal significance for the SRR in Fig. 1 compared with shadow area (5.1) and Rayleigh (6.1) approximations and sum rule bounds. The sum rule bounds have the same slope as the low-frequency asymptotic but shifted to incorporate resonances (6.9) with fractional bandwidth B or a UWB setting (6.10) with onset frequency at ka.

The sum rule (6.2) for the SRR in Fig. 8 is more interesting for a circumscribing geometry such as a planar rectangle with width ℓ and length 2ℓ. Using that the polarizability $\langle\gamma\rangle$ is limited by the high-contrast polarizability for any circumscribing structure [14], we can use the high-contrast polarizability of the rectangle

$$\langle\gamma_\infty\rangle_{\text{rec}} \approx 1.64a^3 \geq \langle\gamma\rangle_{\text{SRR}} \approx 1.55a^3, \tag{6.12}$$

as a limit for the polarizability of all substructures fitting within the rectangular region. The closeness between the polarizabilities for the SRR to the rectangle can be understood by the interpretation of polarizability as the ability of the structure to separate charge, see Box 6, together with charge concentration at the edges implies that removing the inner part of the rectangle has a minor effect on the polarizability.

Fig. 9 compares the total modal significance for three PEC structures fitting within a rectangular shape. The SRR and meander line are dominated by single dipole resonances with $\|\mathbf{T}\|_{\text{F}}^2 \approx 1$ around $ka \approx 0.7$ and $ka \approx 0.6$, respectively. The capacitively-loaded crossed dipole structure has a two modes resonance around $ka \approx 1.1$ with $\|\mathbf{T}\|_{\text{F}}^2 \approx 2$. The low- and high-frequency responses for the circumscribing rectangle are indicated by the dashed lines. Here, it is seen that the high-frequency responses are below the dashed line due to their smaller areas. Similarly, the low-frequency responses are below the dashed curve due to the monotonicity of $\langle\gamma^2\rangle$.

The physical limits for UWB onset frequency and fractional bandwidths $B \in \{0.1, 0.01\}$ are determined from the high-contrast polarizability of the circumscribing rectangle (6.12). They are hence valid for every PEC structure fitting within the rectangle. This observation is valid for all shapes, making it interesting to investigate high-contrast polarizability for other shapes.

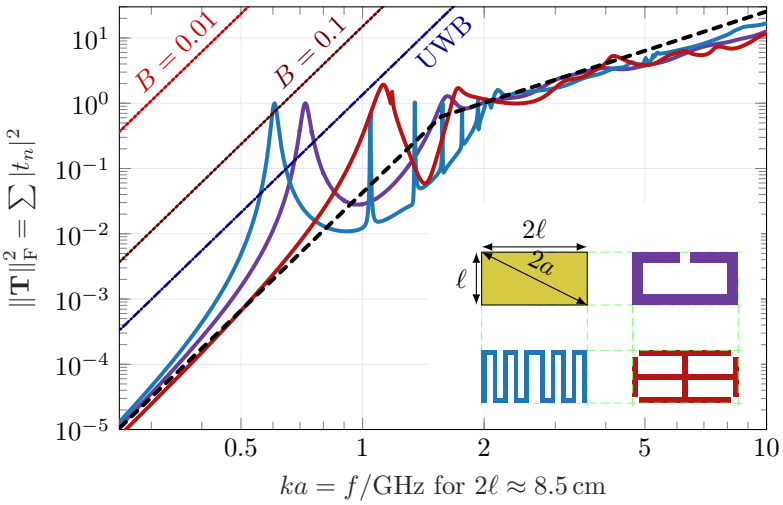

Figure 9: Total modal significances for a SRR, a meanderline, and a dual polarized capped dipole. Performance is compared with physical limits for UWB onset frequency and fractional bandwidths $B \in \{0.1, 0.01\}$.

7 Minimum size for NDoF

The presented analysis demonstrates that the average shadow area $\langle A_{\mathrm{s}} \rangle$ and high contrast polarizability $\langle \gamma_\infty \rangle$ are fundamental parameters to understanding the DoF of arbitrarily shaped objects. Dependence on these parameters for different geometries is hence vital for the estimation of the available NDoF. Fig. 10 depicts normalized parameter values $\langle A_{\mathrm{s}} \rangle / (\pi a^2)$ and $\langle \gamma_\infty \rangle / (4\pi a^3)$ for spheroidal, cylinder, ellipse, and rectangular shapes of varying aspect ratios ℓ_1/ℓ_2. The normalization corresponds to values for a spherical region and produces results bounded by unity. This dominance by the circumscribing sphere can be interpreted as monotonicity of the parameters in the region, *i.e.*, removing region (material) reduces parameter values. For example, a square can be constructed from a circular disc by removing parts close to the edges implying lower parameter values for the square than for the disc.

Average polarizability and shadow area decrease rapidly in the limit $\ell_1/\ell_2 \to 0$, *i.e.*, it is difficult to have high NDoF for needle-shaped objects. Ellipses and rectangles are planar objects and have symmetric parameter values around $\ell_1 = \ell_2$. The average high contrast polarizability of a circular disc is $\langle \gamma_\infty \rangle = 32a^3/9$ and shadow area $\langle A_{\mathrm{s}} \rangle = \pi a^2/2$ as observed for the ellipse with $\ell_1 = \ell_2$ and spheroid and cylinder in the limit $\ell_1/\ell_2 \to \infty$. These results highlight the relatively large difference between needle shapes ($\ell_1/\ell_2 \to 0$) and planar (disc) surfaces ($\ell_1/\ell_2 \to \infty$) and the relatively small difference between discs and sphere. Here, it is important to realize that the analysis for shadow area assumes that the dimension of the object is resolved and hence not of 1D-wire type.

The minimal electrical size for a desired NDoF is estimated from parameters using (5.3) and *e.g.*, (6.10). For example, a larger antenna array may request $N = 50$ significant CM at 5 GHz and using $N \approx 4\pi \langle A_{\mathrm{s}} \rangle / \lambda^2$ with $\lambda \approx 6\,\mathrm{cm}$ gives $\langle A_{\mathrm{s}} \rangle \geq$

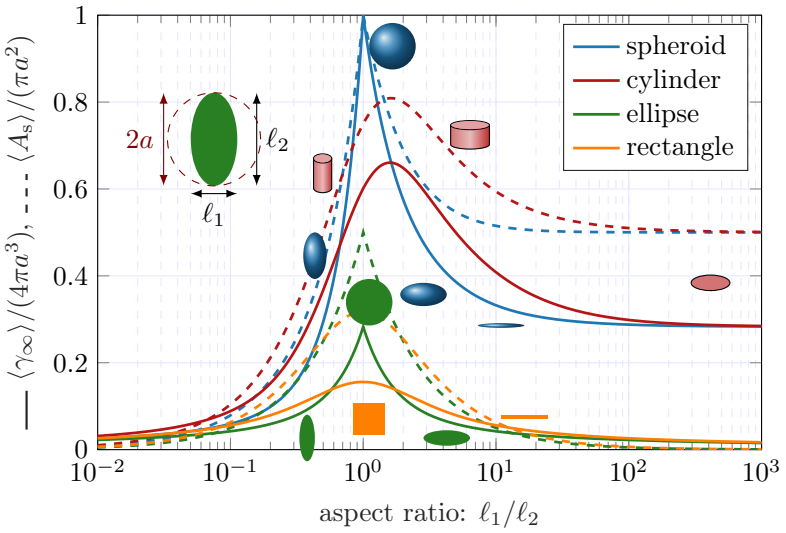

Figure 10: Normalized average high-contrast polarizability $\langle\gamma_\infty\rangle/(4\pi a^3)$ (solid) and average shadow area $\langle A_s\rangle/(\pi a^2)$ (dashed) for spheroids, cylinders, ellipses, and rectangles with aspect ratio ℓ_1/ℓ_2.

143 cm^2, an idea of the physical size of the object through the shadow area. Considering aspect ratio $\ell_1 = \ell_2$, we observe that for cylinders $\langle A_s\rangle \approx 0.75\pi a^2 \Rightarrow a \geq 7.8$ cm and for squares $a \geq 12$ cm. Similarly, we might consider smaller bandwidth-limited (constrained) devices. Using (6.10) an UWB system operating above 5 GHz with $N = 3$ resonant modes has $\langle\gamma_\infty\rangle \geq 3.5$ cm^3 and hence $a \geq 0.8$ cm for the cylinder and $a \geq 1.2$ cm for the square.

These basic parameters provide insight into the potential DoF of an object and complement numerical investigations.

8 Conclusion

In this paper, we have investigated the estimation of degrees of freedom and to this end derived analytic estimates for the number of dominant characteristic modes for arbitrarily shaped objects. It is shown that the NDoF defined in this way is linked, through the average scattering cross-section, to the average shadow area of the object in the electrically large limit and the polarizability in the electrically small regime. This NDoF is determined for a given object and provides typical average values in contrast to the approach in [8, 9] which is based on a bound on all objects within a region. It is always possible to locally modify the geometry to construct resonances at a specific frequency which locally adds DoF at this frequency. Through the forward scattering sum rule we showed how these bandwidth constraints impact the NDoF.

A priori estimates of the NDoF based on the shadow area and polarizability, as presented in this paper, have merit in understanding design spaces and object capability. Moreover, knowledge of the NDoF is useful in computations such as

iterative solvers which can terminate after the sought-for DoFs are found [27].

In this work, we considered objects of non-zero geometrical area, and on the topic of large wire-based arrays with no area, one could consider the solid array aperture as the design region. In this paper we connect, for electrically large structures, the shadow area to scattering and NDoF. Large shadow area relates to large interaction and these array configurations used for maximal gain purposes [23] could be estimated from the maximal shadow area rather than the average. The results in this paper reinterprets the estimate in [23] to that all NDoF are used for a disc but only half if compared with the circumscribing sphere as the disc have half shadow area compared to the sphere, see Box 5.

References

[1] C. F. Bohren and D. R. Huffman. "Absorption and Scattering of Light by Small Particles". John Wiley & Sons, 1983.

[2] O. M. Bucci and G. Franceschetti. "On the degrees of freedom of scattered fields". *IEEE Trans. Antennas Propag.* 37 (7) (1989): pp. 918–926.

[3] M. Cabedo-Fabres, E. Antonino-Daviu, A. Valero-Nogueira, and M. Bataller. "The theory of characteristic modes revisited: a contribution to the design of antennas for modern applications". *IEEE Antennas Propag. Mag.* 49 (5) (2007): pp. 52–68.

[4] M. Capek, J. Lundgren, M. Gustafsson, K. Schab, and L. Jelinek. "Characteristic mode decomposition using the scattering dyadic in arbitrary full-wave solvers". *IEEE Trans. Antennas Propag.* 71 (1) (2023): pp. 830–839.

[5] Y. Chen and C.-F. Wang. "Characteristic Modes: Theory and Applications in Antenna Engineering". John Wiley & Sons, 2015.

[6] G Di Francia. "Directivity, super-gain and information". *IRE Transactions on Antennas and Propagation* 4 (3) (1956): pp. 473–478.

[7] G. T. Di Francia. "Resolving power and information". *Josa* 45 (7) (1955): pp. 497–501.

[8] C. Ehrenborg and M. Gustafsson. "Physical bounds and radiation modes for MIMO antennas". *IEEE Trans. Antennas Propag.* 68 (6) (2020): pp. 4302–4311.

[9] C. Ehrenborg, M. Gustafsson, and M. Capek. "Capacity bounds and degrees of freedom for MIMO antennas constrained by Q-factor". *IEEE Trans. Antennas Propag.* (2021).

[10] M. Franceschetti. "Wave theory of information". Cambridge University Press, 2017.

[11] R. J. Garbacz and R. H. Turpin. "A generalized expansion for radiated and scattered fields". *IEEE Trans. Antennas Propag.* 19 (3) (1971): pp. 348–358.

[12] M. Gustafsson. "Time-domain approach to the forward scattering sum rule". *Proc. R. Soc. A* 466 (2010): pp. 3579–3592.

[13] M. Gustafsson, C. Sohl, and G. Kristensson. "Illustrations of new physical bounds on linearly polarized antennas". *IEEE Trans. Antennas Propag.* 57 (5) (2009): pp. 1319–1327.

[14] M. Gustafsson, C. Sohl, and G. Kristensson. "Physical limitations on antennas of arbitrary shape". *Proc. R. Soc. A* 463 (2007): pp. 2589–2607.

[15] M. Gustafsson. *AntennaQ—MATLAB script that computes physical bounds on Q and D/Q for antennas.* http://www.mathworks.se/matlabcentral/fileexchange/26806-antennaq. 2010.

[16] M. Gustafsson, L. Jelinek, K. Schab, and M. Capek. "Unified theory of characteristic modes: part I–fundamentals". *IEEE Trans. Antennas Propag.* 70 (12) (2022): pp. 11801–11813.

[17] M. Gustafsson, D. Tayli, and M. Cismasu. "Physical bounds of antennas". In: *Handbook of Antenna Technologies.* Ed. by Z. N. Chen. Springer-Verlag, 2015, pp. 197–233.

[18] K. Haneda, A. Khatun, M. Dashti, T. A. Laitinen, V.-M. Kolmonen, J.-I. Takada, and P. Vainikainen. "Measurement-based analysis of spatial degrees of freedom in multipath propagation channels". *IEEE Trans. Antennas Propag.* 61 (2) (2012): pp. 890–900.

[19] J. E. Hansen, ed. "Spherical Near-Field Antenna Measurements". IEE electromagnetic waves series 26. Peter Peregrinus Ltd., 1988.

[20] R. F. Harrington and J. R. Mautz. "Theory of characteristic modes for conducting bodies". *IEEE Trans. Antennas Propag.* 19 (5) (1971): pp. 622–628.

[21] J. D. Jackson. "Classical Electrodynamics". Third. John Wiley & Sons, 1999.

[22] R. Janaswamy. "On the EM degrees of freedom in scattering environments". *IEEE Trans. Antennas Propag.* 59 (10) (2011): pp. 3872–3881.

[23] P.-S. Kildal, E. Martini, and S. Maci. "Degrees of freedom and maximum directivity of antennas: a bound on maximum directivity of nonsuperreactive antennas". *IEEE Antennas and Propagation Magazine* 59 (4) (2017): pp. 16–25.

[24] R. E. Kleinman and T. B. A. Senior. "Rayleigh scattering". In: *Low and high frequency asymptotics.* Ed. by V. V. Varadan and V. K. Varadan. Vol. 2. Handbook on Acoustic, Electromagnetic and Elastic Wave Scattering. Elsevier Science Publishers, 1986. Chap. 1, pp. 1–70.

[25] G. Kristensson. "Scattering of Electromagnetic Waves by Obstacles". SciTech Publishing, an imprint of the IET, 2016.

[26] H. Li, Z. T. Miers, and B. K. Lau. "Design of orthogonal MIMO handset antennas based on characteristic mode manipulation at frequency bands below 1 GHz". *IEEE Trans. Antennas Propag.* 62 (5) (2014): pp. 2756–2766.

[27] J. Lundgren, K. Schab, M. Capek, M. Gustafsson, and L. Jelinek. "Iterative calculation of characteristic modes using arbitrary full-wave solvers". *IEEE Antennas Wireless Propag. Lett.* 22 (4) (2023): pp. 799–803.

[28] M. D. Migliore. "On the role of the number of degrees of freedom of the field in MIMO channels". *IEEE Trans. Antennas Propag.* 54 (2) (2006): pp. 620–628.

[29] M. Migliore. "On electromagnetics and information theory". *IEEE Trans. Antennas Propag.* 56 (10) (2008): pp. 3188–3200.

[30] R. E. Peierls. "Surprises in Theoretical Physics". Princeton University Press, 1979.

[31] R. Piestun and D. A. Miller. "Electromagnetic degrees of freedom of an optical system". *JOSA A* 17 (5) (2000): pp. 892–902.

[32] A. Pizzo, A. de Jesus Torres, L. Sanguinetti, and T. L. Marzetta. "Nyquist sampling and degrees of freedom of electromagnetic fields". *IEEE Transactions on Signal Processing* 70 (2022): pp. 3935–3947.

[33] A. S. Poon, R. W. Brodersen, and D. N. Tse. "Degrees of freedom in multiple-antenna channels: a signal space approach". *IEEE Transactions on Information Theory* 51 (2) (2005): pp. 523–536.

[34] D. M. Pozar. "Microwave Engineering". John Wiley & Sons, 1998.

[35] E. M. Purcell. "On the absorption and emission of light by interstellar grains". *J. Astrophys.* 158 (1969): pp. 433–440.

[36] C. Sohl and M. Gustafsson. "A priori estimates on the partial realized gain of Ultra-Wideband (UWB) antennas". *Quart. J. Mech. Appl. Math.* 61 (3) (2008): pp. 415–430.

[37] C. Sohl, M. Gustafsson, and G. Kristensson. "Physical limitations on broadband scattering by heterogeneous obstacles". *J. Phys. A: Math. Theor.* 40 (2007): pp. 11165–11182.

[38] J. Song and W. C. Chew. "Error analysis for the truncation of multipole expansion of vector Green's functions". *IEEE microwave and wireless components letters* 11 (7) (2001): pp. 311–313.

[39] J. A. Stratton. "Electromagnetic Theory". McGraw-Hill, 1941.

[40] V Vouk. "Projected area of convex bodies". *Nature* 162 (4113) (1948): pp. 330–331.